Underway pCO$_2$ surveys unravel CO$_2$ invasion of Lake Superior from seasonal variability

D. E. Sandborn[1,2], E. C. Minor[1,3]

[1]Large Lakes Observatory, University of Minnesota Duluth, Duluth MN 55812 USA
[2]Water Resources Science Program, University of Minnesota, St. Paul, MN 55108 USA
[3]Department of Chemistry and Biochemistry, University of Minnesota Duluth, Duluth, MN 55812 USA

Key Points:

- Underway pCO$_2$ was measured in Lake Superior from 2019 to 2022 to form the first multi-year pCO$_2$ time series in the Laurentian Great Lakes.
- The seasonal pCO$_2$ cycle illustrated competition of thermal and biophysical drivers and spatial heterogeneity associated with riverine influence.
- Lake Superior maintained atmospheric CO$_2$ equilibrium leading to increasing surface water pCO$_2$ on decadal timescales.

Corresponding author: Daniel E. Sandborn, `sandb425@umn.edu`

Abstract

This study observed seasonal trends and inferred drivers of CO_2 biogeochemistry at the air-water interface of Lake Superior. Underway carbon dioxide partial pressure (pCO_2) was measured in surface water during 69 transects spanning ice free seasons of 2019-2022. These data comprise the first multiannual pCO_2 time series in the Laurentian Great Lakes. Surface water pCO_2 was closely tied to increasing atmospheric pCO_2 by a 100 day CO_2 equilibration timescale, while seasonal variability was controlled equally by thermal and biophysical drivers during the ice-free season. Comparison to previous modeling efforts indicates that Lake Superior surface pCO_2 increased at a similar rate as the atmosphere over the preceding two decades. Spatial heterogeneity in CO_2 dynamics was highlighted by a salinity-based delineation of "riverine" and "pelagic" regimes, each of which displayed a net CO_2 influx over Julian days 100-300 on the order of 30 Gmol C. These findings refine previous estimates of Lake Superior C fluxes, support predictions of anthropogenic CO_2 invasion, point to new observation strategies for large lakes, and highlight an urgent need for studies of changes to lacustrine C cycling.

Plain Language Summary

Carbon dioxide gas concentrations were measured in surface waters of Lake Superior for four years, forming the first multi-year dataset of direct observations of carbon dioxide gas concentration in the Laurentian Great Lakes. Lake Superior's surface carbon dioxide concentration was closely tied to that of the atmosphere on time scales longer than one year. Seasonal variations in carbon dioxide concentration were driven by water temperature, biological activity, river influence, and gas exchange with the atmosphere. Lake Superior released and absorbed carbon dioxide cyclically at different times of the year, absorbing more than it released from April to November. Mixing surface waters maintain the same carbon dioxide concentration as the atmosphere (which is increasing due to anthropogenic emissions), so the partial pressure of carbon dioxide gas in Lake Superior surface waters increased over the past two decades. This work improves the scientific understanding of carbon cycling in Lake Superior and advances techniques for carbon cycle observation and modeling of other lakes.

1 Introduction

Measurements of carbon cycling in the Earth's hydrosphere are central to understanding global biogeochemical cycling and responses to perturbation (Le Quéré et al., 2013). Continuing anthropogenic emissions of carbon dioxide (CO_2) are increasing atmospheric concentrations at an unprecedented rate, which may force changes in carbonate equilibria in the oceans (Feely et al., 2001), in soils (Oh & Richter, 2004), in rivers (Raymond & Hamilton, 2018), and in lakes (Alin & Johnson, 2007).

Many studies of the inorganic C system in inland waters collect and analyze discrete water samples for parameters including pH, dissolved inorganic carbon (DIC), total alkalinity (A_T), and partial pressure of carbon dioxide (pCO_2) (Cole et al., 1994). Direct measurements of CO_2 flux across the air-water interface are also collected via floating chamber or eddy covariance methods (Podgrajsek et al., 2014). Constructing time series of discrete water chemistry measurements is time- and labor-intensive and may not resolve the high spatial and temporal variability of inorganic C cycling in many water bodies such as large lakes with high spatial and temporal variability (Schilder et al., 2013). Additionally, calculation of one inorganic C parameter from two others remains fraught with uncertainty due to ongoing challenges associated with measurement and equilibrium calculations in freshwater (Liu et al., 2020; Minor & Brinkley, 2022; Young et al., 2022). To bridge these gaps in observational capabilities, instruments measuring inorganic C parameters continuously or autonomously have been developed and deployed in aquatic systems spanning the lacustrine-marine spectrum (Bushinsky et al., 2019; Lynch et al., 2010). Recent years have seen applications of pH and pCO_2 underway sensors that perform with uncertainties similar to those of discrete sample measurements (Ma et al., 2019; Takeshita et al., 2018).

Inorganic C chemistry remains less-studied in inland waters than in marine systems (Phillips et al., 2015), due in part to high physical, chemical, biological, and temporal heterogeneity within and among lakes and rivers. Large lakes may serve as stepping-stones for application and further development of oceanographic chemical techniques in inland waters. Their great volume and relatively small terrestrial influences lend them a more constant chemistry and physics than their smaller peers. The largest of lakes share with oceans similar biogeochemical features and relative importance to local and global biogeochemical cycling (Sterner et al., 2017). On the other hand, large lakes respond more rapidly than the global ocean to perturbation; their hydrologic residence times (c. 190 years for Lake Superior) are shorter than that of the global ocean (millennia). Holomictic lakes experience full water column mixing at least annually, which represents a homogenizing driver not observed in oceans. For these reasons, large lakes can act as test systems for investigations of environmental variables, with responses occurring on more accessible spatial and temporal scales for research (Sterner, 2021).

The Laurentian Great Lakes lie on the border of the United States of America and Canada and within the historical and contemporary lands of Native American and First Nations. They constitute the largest contiguous aquatic ecosystem on Earth (Wetzel, 2001), yet C cycling in the Great Lakes is not well-understood (Minor & Oyler, 2021). It remains unclear to what extent the Great Lakes are net sources or sinks of CO_2 to the atmosphere (McDonald et al., 2013; N. Urban & Desai, 2009). Alin and Johnson (2007) concluded that they are annual net CO_2 sources, while Bennington et al. (2012) noted that studies of CO_2 cycling in Lake Superior have been biased by sparse observations restricted to the ice-free period, and could not "close the cycle" by modeling all C inputs and outputs. These pioneering studies were confounded by observations of inorganic C cycling that were sparse, irregular or unrepresentative of the lakes as a whole. This situation is similar to that of the Southern Ocean or South Pacific Ocean, in which limited observation hindered attempts to constrain biogeochemical budgets (Takahashi et al., 2009). Such lakes functioning as "sentinels, integrators, and

97 regulators of climate change" (Williamson et al., 2009) exert significant influence on
98 regional and global C budgets (Cole, 2013) and demand more detailed study.

99   This research focuses on surface water $p\mathrm{CO_2}$ variations over time and space
100 to illustrate the C cycle of Lake Superior in unprecedented detail. $p\mathrm{CO_2}$ in water
101 responds to physical (temperature, pressure, salinity), chemical (pH, DIC, $\mathrm{A_T}$, $\mathrm{CaCO_3}$
102 dissolution/precipitation), and biological (production, respiration) drivers (Zeebe &
103 Wolf-Gladrow, 2001), such that a comprehensive understanding of $p\mathrm{CO_2}$ variability
104 sheds light on a suite of biogeochemical functions. As a direct driver of $\mathrm{CO_2}$ flux across
105 the air/water interface, $p\mathrm{CO_2}$ in surface waters acts as an important parameter of
106 atmospheric $\mathrm{CO_2}$ accumulation. Accurate predictions of climate change and mitigation
107 efforts require an improved understanding of the role of waters bodies as sources and
108 sinks of $\mathrm{CO_2}$ and other greenhouse gases (Cavallaro et al., 2018).

109   Lake Superior has a small surface area-to-catchment ratio of 1.55 (Urban, 2005)
110 and is underlain by a weathering-resistant igneous mineralogy leading to exceptionally
111 dilute, soft, and carbonate-poor water chemistry. Its water is warming faster than
112 the overlying atmosphere (Austin & Colman, 2008), and the concentration of most of
113 its major ions is increasing (Chapra et al., 2012). Interannual trends in $\mathrm{A_T}$, pH, and
114 $p\mathrm{CO_2}$ have proven difficult to constrain due to covariation with lake level, influence
115 from Dreissenid calcification in tributaries, large measurement uncertainty, and spatial
116 heterogeneity (Minor & Brinkley, 2022). These poorly-understood changes contribute
117 to the need for a sustained campaign of spatially- and temporally-comprehensive mea-
118 surements of the inorganic carbon system in Lake Superior.

119   In this work, underway $p\mathrm{CO_2}$ measurements gathered by instrumentation aboard
120 *RV Blue Heron* from four consecutive field seasons (April-November 2019-2022) pro-
121 vided a survey of unprecedented spatial and temporal scope describing inorganic C
122 cycling drivers and variability in a large lake. This information was used to infer
123 trends in $p\mathrm{CO_2}$ and $\mathrm{CO_2}$ flux over space and time and establish the interplay of ther-
124 mal and biophysical drivers of $p\mathrm{CO_2}$, and compare the relative magnitudes of wind
125 velocity and $p\mathrm{CO_2}$ saturation as drivers of $\mathrm{CO_2}$ flux. The results demonstrate a path-
126 way towards comprehensive $\mathrm{CO_2}$ budgets for the Laurentian Great Lakes via novel
127 observation strategies and improved modeling efforts.

2 Methods

129   Underway instrument datasets from 69 transects of the RV Blue Heron were
130 compiled. These efforts included single-day endeavors near the vessel's home port
131 of Duluth Minnesota, as well as multi-week transects across the Laurentian Great
132 Lakes (Figure 1). Water was directed from the ship's water intake line at 2 m depth
133 through a suite of sensors measuring parameters including dry molar fraction of carbon
134 dioxide ($\mathrm{xCO_2}$), sea surface temperature (SST), and sea surface conductivity. These
135 were combined with wind velocity, barometric pressure, and air temperature collected
136 from an onboard meteorological station. The multi-year span considered in this study
137 permits evaluation of interannual variability in inorganic C biogeochemistry despite
138 limited cruises in 2020 and 2021 due to challenges associated with the Coronavirus
139 pandemic.

140     $\mathrm{xCO_2}$ was measured in water from the underway system at 2 second intervals
141 using a Sunburst Sensors SuperCO2 instrument equipped with a showerhead equili-
142 brator. Measurements from four standard gases with $\mathrm{CO_2}$ concentrations between 0
143 and 1018 ppm were performed every 2 hours (Supplementary Figure S1) and the 60
144 seconds before and after calibration removed from the time series to prevent memory
145 effects. The slope and intercept values from a type-I linear regression of measured
146 vs. standard $\mathrm{xCO_2}$ were used to correct surface water $\mathrm{xCO_2}$ before conversion to

$p\text{CO}_2$ (Equation 1) A nearly-identical instrument demonstrated a $p\text{CO}_2$ measurement uncertainty of ± 5 µatm (M. DeGrandpre et al., 2020). SST and conductivity were obtained from a SBE21 thermosalinograph every 2 seconds. Conductivity was converted to practical salinity using the equations of Hill et al. (1986). Wind velocity was measured with a Young 05106 wind monitor on a mast 10 meters from the sea surface. Air temperature was obtained from a Young 41372VC thermometer. It was assumed that mast-measured windspeed (corrected for travel) approximated neutral wind speed at 10 meters (U_{10n}) sufficiently well for the parameterization of instantaneous CO_2 flux. Measured $p\text{CO}_2$ and calculated CO_2 flux were averaged for each day of each transect in $0.01° \times 0.01°$ boxes (approximately 1.1 x 0.8 km at the latitude of Lake Superior) to normalize distributions of $p\text{CO}_2$ and CO_2 flux on an areal basis and prevent biases due to vessel idling.

$p\text{CO}_2$ was calculated as a product of ambient atmospheric pressure (p_{atm}) and xCO_2 both measured by the SuperCO2 instrument and corrected for water vapor partial pressure ($p_{\text{H}_2\text{O}}$) calculated as a function of temperature assuming saturation (Dickson et al., 2007):

$$p\text{CO}_2 = \text{xCO}_2 \cdot (p_{\text{atm}} - p_{\text{H}_2\text{O}}) \tag{1}$$

CO_2 flux was parameterized by the difference between aqueous and atmospheric $p\text{CO}_2$, multiplied by the gas transfer velocity (k), a function of Schmidt number Sc (Ho et al., 2006), mean squared neutral wind speed at 10 meters above the sea surface ($< U_{10\,n}^2 >$), and K_o, the solubility of CO_2 in water (Weiss, 1974). Positive values of CO_2 flux indicate efflux.

$$\text{CO}_2 \text{ Flux} = kK_o\left(p\text{CO}_{2\text{ aq}} - p\text{CO}_{2\text{ atm}}\right) \tag{2}$$

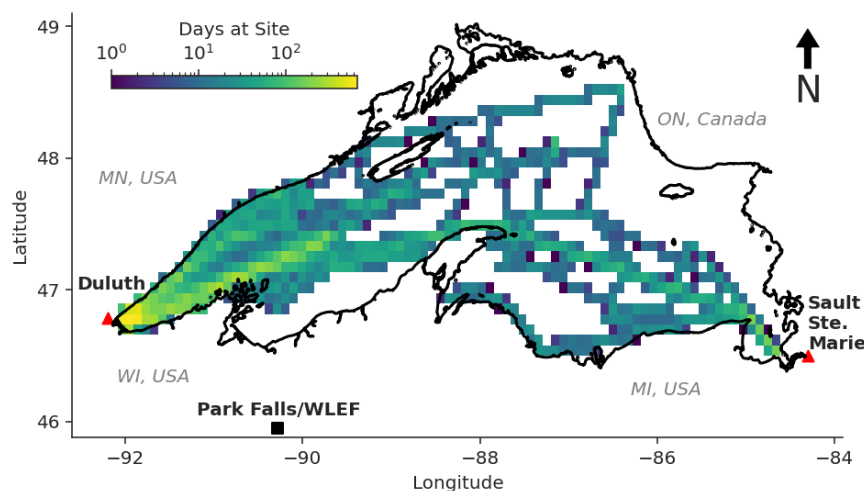$$k = 0.266 < U_{10}^2 > \left(\frac{Sc}{600}\right)^{-0.5} \tag{3}$$

We compared two sources of atmospheric CO_2 concentrations for calculation of CO_2 flux: underway-measured atmospheric $p\text{CO}_2$ measured every 2 hours by the SuperCO2 instrument and atmospheric $p\text{CO}_2$ as measured at the WLEF/Park Falls Wisconsin tower (A. Desai, 2022). The WLEF/Park Falls time series was chosen for flux calculations, as detailed in the Results.

There is considerable disagreement among gas flux parameterizations applied to lakes. Previous studies have assumed no wind dependence (Cole & Caraco, 1998) or different values of the empirical coefficient of the gas transfer velocity equation (Atilla et al., 2011). The parameterization in this study (Ho et al., 2006) was chosen on the grounds that Lake Superior can be understood similarly to marine environments, with a high range of wind speeds and large fetch which merit the quadratic wind dependence discussed by Wanninkhof (1992) (D. Ho, personal communication).

Calculations were completed with Python 3.8, using Pandas (Reback et al., 2022) for data structure manipulation, SciPy (Virtanen et al., 2020) and Statsmodels (Seabold & Perktold, 2010) for regression and statistical analysis, Numpy (Harris et al., 2020) for array computation, PyCO$_2$SYS (Humphreys et al., 2020) for CO_2 system calculations, GSW-Python (Firing et al., 2021) for salinity conversions, and Matplotlib (Hunter, 2007) and Seaborn (Waskom, 2021) for visualization.

3 Results

More than 6×10^6 measurements of xCO_2 in Lake Superior surface waters were assembled into a $p\text{CO}_2$ and CO_2 flux timeseries. These data spanned the lake's most significant hydrological regions, including shallow coastal zones, deep (maximum 406

Figure 1. Underway measurement density transects 2019-2022, visualized as the number of occupations of approximately 5 km squares. The number of days of observation ranged from 0 to nearly 600. The cities of Duluth and Sault Ste. Marie, between which multi-lake transects traverse, are indicated by red triangles. The Park Falls/WLEF tower is denoted by a black square.

m) waters, riverine outlets, and regions bordering significant human development (Figure 1). The most heavily-observed regions included the far western arm of Lake Superior and a cross-lake transect from Duluth to Sault Ste. Marie. Binning of $p\text{CO}_2$ and CO_2 flux data by grouping observations by date and 0.01° boxes yielded 1.3×10^4 observations.

3.1 Underway Timeseries Overview

Mean observed SST was 11.4 °C with a median of 12.7 °C. SST varied widely among and within cruises, ranging from a maximum of 23.5 °C in July 2019 near the center of the Far Western Arm to a minimum of 0.45 °C in April 2022 in the plume of the St. Louis River Estuary. Practical salinity calculated from conductivity ranged from a near-constant 0.0446 in unstratified offshore waters to values exceeding 0.09 in the plume of the St. Louis River Estuary, displaying a mean of 0.0455, a median of 0.0454, and a standard deviation of 0.0015. The timing of thermal stratification in Lake Superior varied widely among locations and years (Austin et al., 2022), so observations within 0.5 °C of the temperature of maximum density of freshwater (3.98 °C) were designated as unstratified. Stratification occurred between late June and August, depending on year and location (Figure 2a); interannual weather variability exerted considerable influence on stratification development, as indicated by the historically late stratification of Lake Superior in August 2022 (J. Austin, personal communication).

Surface-water DIC and pH (free scale) were calculated from measured $p\text{CO}_2$, SST, and an assumed A_T of 840 µmol kg^{-1} (Figure 2d-e) with PyCO$_2$SYS, using the carbonate constants of Waters et al. (2014). A_T is largely invariant in Lake

Superior (Minor and Brinkley 2022, Sandborn et al. 2023) except in regions with significant terrestrial influence; no AT-conductivity relationship for Lake Superior has been published, so AT was not parameterized by underway data. Calculated pH_{free} exhibited a mean of 8.075 and standard deviation of 0.093, while calculated DIC exhibited a mean of 855.0 µmol kg^{-1} and standard deviation of 8.8 µmol kg^{-1}. This pH_{free} distribution fell within the range of values given in Minor and Brinkley (2022), while the mean calculated DIC was 10-40 µmol kg^{-1} higher than observations given in Zigah et al. (2011) and Sandborn et al. (2023). The discrepancy may be due to interannual DIC increases, sampling bias in the latter two studies favoring regions or periods of lower DIC, interferences due to organic alkalinity, or uncertainty associated with equilibrium calculation, all of which remain active areas of research (Minor & Brinkley, 2022; Sandborn et al., 2023). Seasonal variation in DIC was evident as a summertime decrease on the order of 20 µmol kg^{-1}, followed by an autumn increase of c. 10 µmol kg^{-1}.
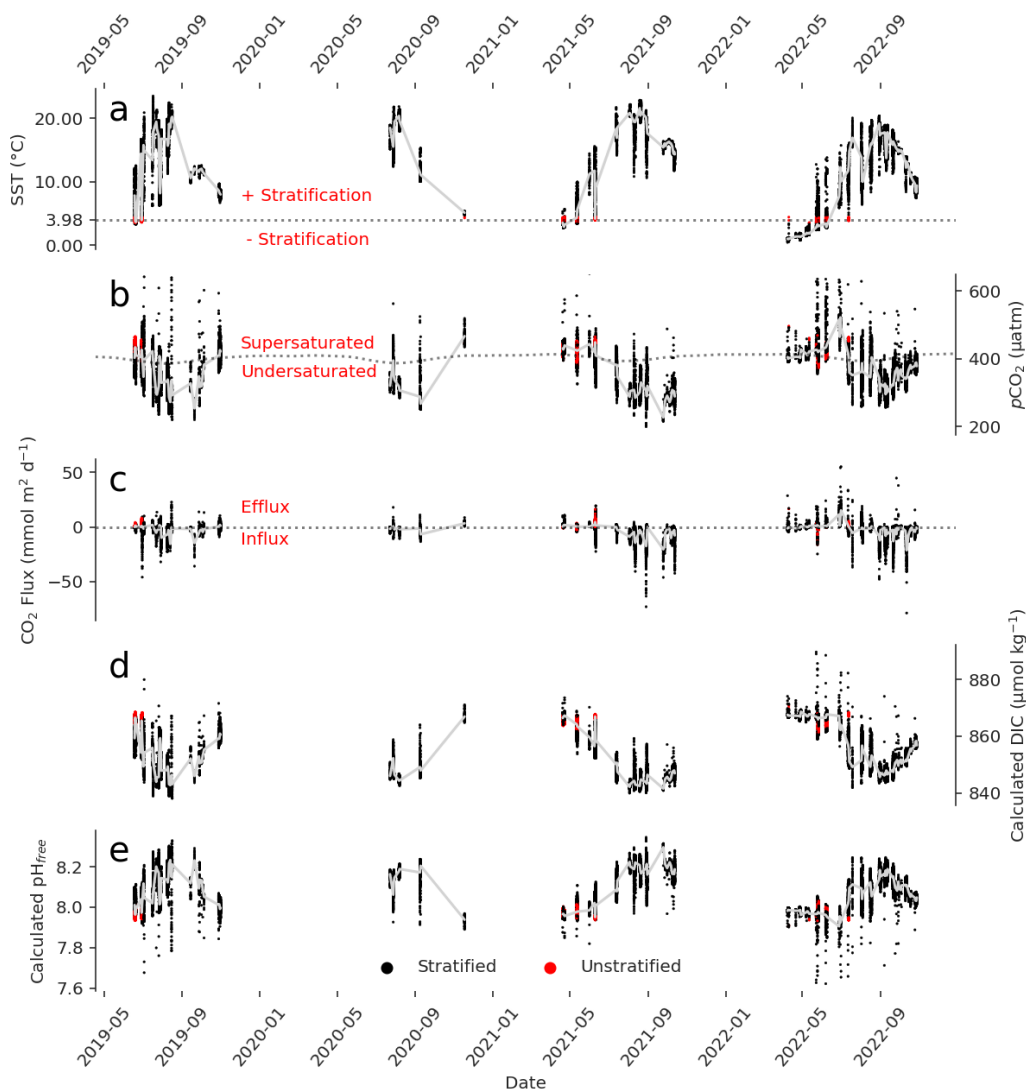
3.2 Atmospheric CO_2

The daily mean shipboard atmospheric xCO_2 varied seasonally in concert with the CO_2 timeseries observed at the Park Falls/WLEF tower (Desai, 2022) (Figure S5), approximately 80 km south of Chequamegon Bay, Wisconsin. Both series displayed a larger annual variability and a phase shift from the Mauna Loa CO_2 time series (Keeling & Keeling, 2017). No systematic biases in atmospheric CO_2 concentration were observed between the underway and Park Falls/WLEF time series within years, yet the underway atmospheric signal displayed a much larger variability. Several anomalies emerged in the underway atmospheric data. Atmospheric xCO_2 measurements in several cruises were consistently higher than expected despite nominal measurements of standard gases and sea surface xCO_2. These cruises included extended periods of idling, and presumably detection of exhaust CO_2 by the underway system. In another two cruises in September 2022, atmospheric (but not sea surface) xCO_2 was depressed over a period of weeks for reasons related to a filter on the air inlet. Due to these discrepancies, we chose to use daily means of nearby Park Falls/WLEF tower hourly measurements of atmospheric xCO_2 with the expectation of a well-mixed atmosphere over these scales. The occurrence of most atmospheric underway xCO_2 measurements within a close approximation of the Park Falls/WLEF timeseries validated this expectation.

3.3 Wind Speed

Wind speed observed on Lake Superior (corrected for direction of travel) exhibited a skewed unimodal distribution with a peak at 4.5 m s^{-1} (Supporting Figure S2a). Some bias may have been incurred by intentional planning of transects around inclement weather and targeting the ice-free season, so it was unclear how well these transects represented the true distribution of wind velocity above Lake Superior. The underway-observed wind speed distribution in 2020 stood out from other years with a lower and irregular distribution; these transects were limited in time and space (Figure S1) and are less likely to represent the true distribution of wind speed over Lake Superior. Comparison of the underway wind speed distributions with those measured offshore at the Stannard Rock Lighthouse over the same periods (Figure S2b) indicates that the underway-observed wind speed distribution closely approximated that of the whole season.

The wind speed distribution peaks observed from either source were lower than the global U_{10n} distribution peak of approximately 7 m s^{-1} in Yang et al. (2022), which may imply an underestimation of CO_2 flux as parameterized by dual-tracer models as in this research. The present scarcity of research on gas flux parameterization validity in large lake systems for which size, morphometry, and variable winds greatly influence

Figure 2. Sea surface temperature, pCO$_2$, calculated CO$_2$ flux, calculated DIC, and calculated pH$_{\text{free}}$ observed in 0.01° boxes on transects of Lake Superior, 2019-2022. Median values for each day of observation are connected by a grey line. **a.** The 3.98 °C temperature of maximum density is indicated by a dotted line, along which lie unstratified conditions, highlighted in red. Depressed springtime surface temperatures of 2022 are visible as a delayed warming trend. **b.** The Park Falls/WLEF time series is displayed as a dotted line separating observations of CO$_2$ supersaturation and undersaturation. **c.** The division of CO$_2$ efflux vs. influx is indicated by a dotted line. **d.** DIC as calculated from pCO$_2$ and assumed A$_T$ = 840 μmol kg^{-1}. **e.** pH (free scale) as calculated from pCO$_2$ and assumed A$_T$ = 840 μmol kg^{-1}.

gas flux magnitude and timing (Perolo et al., 2021; Schilder et al., 2013) does not yet allow exploration of similar biases in this research.

Gas transfer velocities (k) calculated from the underway wind distribution displayed a mean of 1.6 m d^{-1}, about half the mean ocean value of 3.3 m d^{-1} given by Broecker and Peng (1982) and supported by revised gas transfer velocity parameterizations (e.g. Ho et al., 2006; Wanninkhof, 2014). Given this information, along with the 147 m mean depth of Lake Superior (Fuller & Shear, 1995), its Revelle Factor (RF), DIC, and aqueous CO_2 concentration $[CO_2^*]$ (from equilibrium calculations), the characteristic timescale, or e-folding time, of CO_2 equilibration in Lake Superior (τ_{CO_2}) can be estimated (Zeebe & Wolf-Gladrow, 2001):

$$\tau_{CO_2} = \frac{\text{mixing depth}}{k} \cdot \frac{\text{DIC}}{[CO_2^*]} \cdot \frac{1}{RF} \tag{4}$$

During unstratified periods, mean RF was 26.9 $\pm$ 0.6, mean DIC was 867.0 $\pm$ 0.9 µmol kg^{-1}, and mean $[CO_2^*]$ was 29.6 $\pm$ 0.8 µmol kg^{-1} (all $\pm$ s.d.). The resulting τ_{CO_2} during the unstratified period was 100. $\pm$ 4 days; this period is much smaller than that of most of the surface ocean mixed layer, indicating relatively fast CO_2 equilibrium despite Superior's deeper mixed layer. This period is similar in magnitude to the duration of the twice-annual unstratified periods in December-January and May-July (though stratification phenology varies among years; Austin and Colman (2008); Woolway et al. (2021)), so it is reasonable to expect that on multiannual timescales, Lake Superior maintains near-atmospheric CO_2 equilibrium. This inference depends on lake stratification and wind velocity, both of which may shift with the changing climate (Xue et al., 2022). Climate change effects on lake thermal state and atmospheric circulation are likely to have complex effects on lake biogeochemistry which extend to CO_2 flux behavior changes (A. R. Desai et al., 2009).
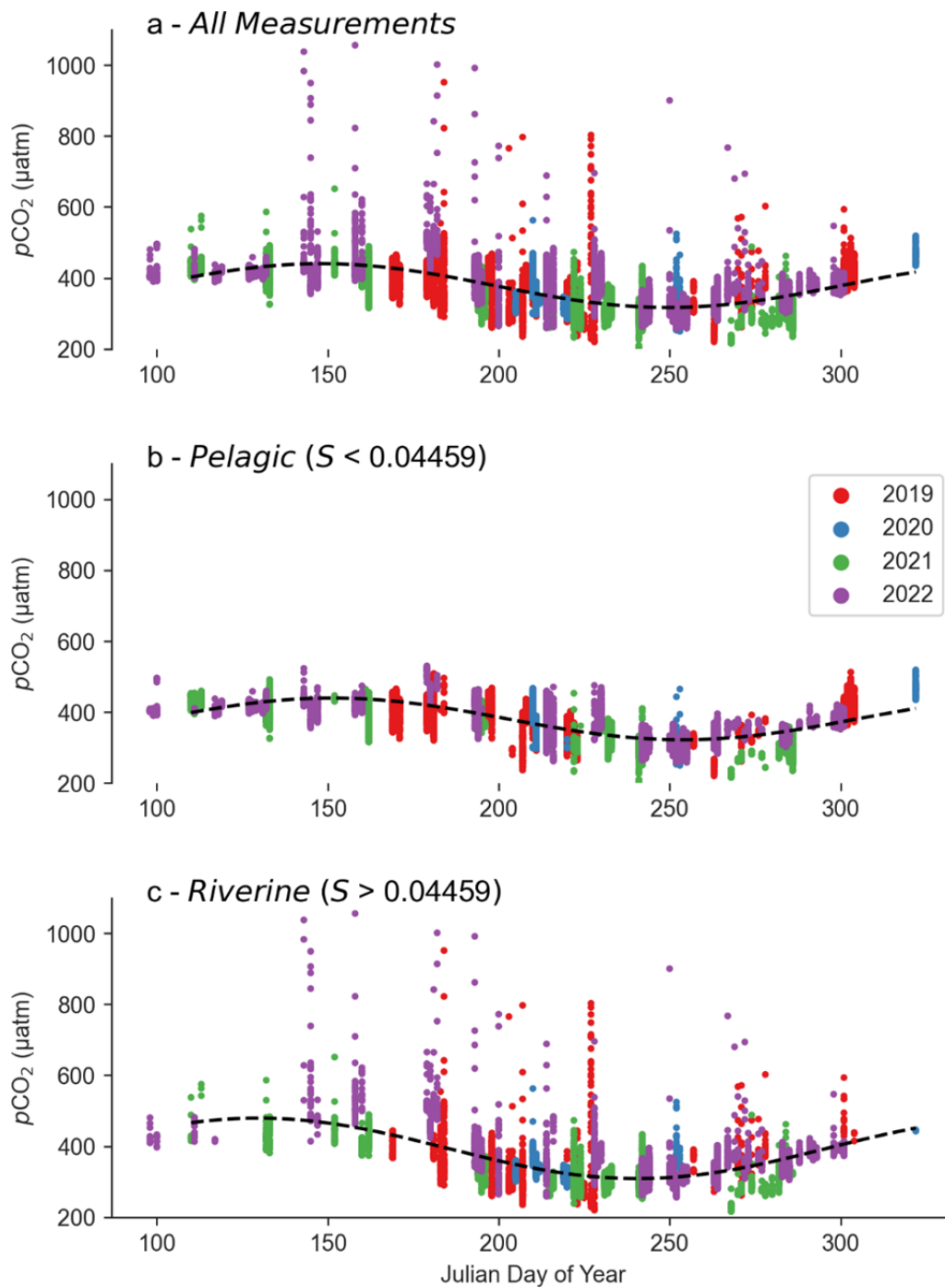
3.4 $p\text{CO}_2$ Variability

A continuous multiannual cycle of observed $p\text{CO}_2$ could not be constructed due to large gaps in the time series, so a synthesized cycle was constructed by combining four years of observations into one based on Julian day of year (DOY). Least-squares regression of observations grouped by 0.01° boxes and date of observation to an equation of the form

$$p\text{CO}_2 = a \cdot sin\left(b \cdot \frac{c - \text{DOY}}{365.25} \right) + d \tag{5}$$

(where a, b, c, and d are regression coefficients) exhibited an amplitude (a) of 58.50 $\pm$ 0.14 µatm and a baseline $p\text{CO}_2$ (d) of 381.197 $\pm$ 0.063 µatm (uncertainty as standard errors of regression coefficients) (Figure 3a)

Spatial heterogeneity was visible in the range of $p\text{CO}_2$ values observed on a given date, with super- and under-saturated conditions observed throughout the year. This high degree of spatial heterogeneity obscured the seasonal cycle of $p\text{CO}_2$ in the lake as a whole. Additionally, the high concentration of transects in the riverine-influenced Western Arm of Lake Superior may not have represented open-water conditions prevailing in the remainder of the lake. Diel variability was examined as a potential source of bias, but no significant difference between daytime and nighttime $p\text{CO}_2$ was found (see Supporting Information).

Confounded spatial and seasonal variabilities were partly separated by salinity into "riverine" and "pelagic" regimes in order to isolate open-water seasonal variability. A cutoff salinity value was defined by statistically significant departure from the surface salinity distribution observed in unstratified periods. In every year of observation, springtime unstratified surface salinity observations formed a narrow distribution

Figure 3. $p\mathrm{CO}_2$ observations grouped by $0.01°$ squares and date during transects of Lake Superior for a synthetic annual time series 2019-2022. Black dashed lines represent sinusoidal regressions of each time series.

315 with a mean of 0.04455 and a standard deviation of 0.00044. This value was taken
316 to represent the mean salinity of the well-mixed lake. Observations with salinity 3
317 standard deviations greater than the unstratified period mean were considered river-
318 influenced. This scheme decreased the noise around the seasonal trend of surface
319 water $p\mathrm{CO}_2$ in pelagic observations (Figure 3b) and highlighted spatial heterogeneity
320 in riverine-influenced observations (Figure 3c). Potential interferences with this clas-
321 sification included evaporation and precipitation, which would be expected to increase
322 and decrease surface salinity, respectively. For this reason, we elected not to construct
323 any quantitative mixing relationship based on underway-measured surface salinity and
324 merely used it as a rough proxy for riverine influence. In pelagic waters of Lake Supe-
325 rior during April-November the mean observed $p\mathrm{CO}_2$ was 380 µatm with a standard
326 deviation of 53 µatm, while in river-influenced waters, the mean observed $p\mathrm{CO}_2$ was
327 343 µatm with a standard deviation of 38 µatm; the depression of riverine regime mean
328 $p\mathrm{CO}_2$ may have been due to promotion of primary production and CO_2 drawdown in
329 nutrient-rich riverine-influenced Lake Superior waters (Minor et al., 2014; Sterner et
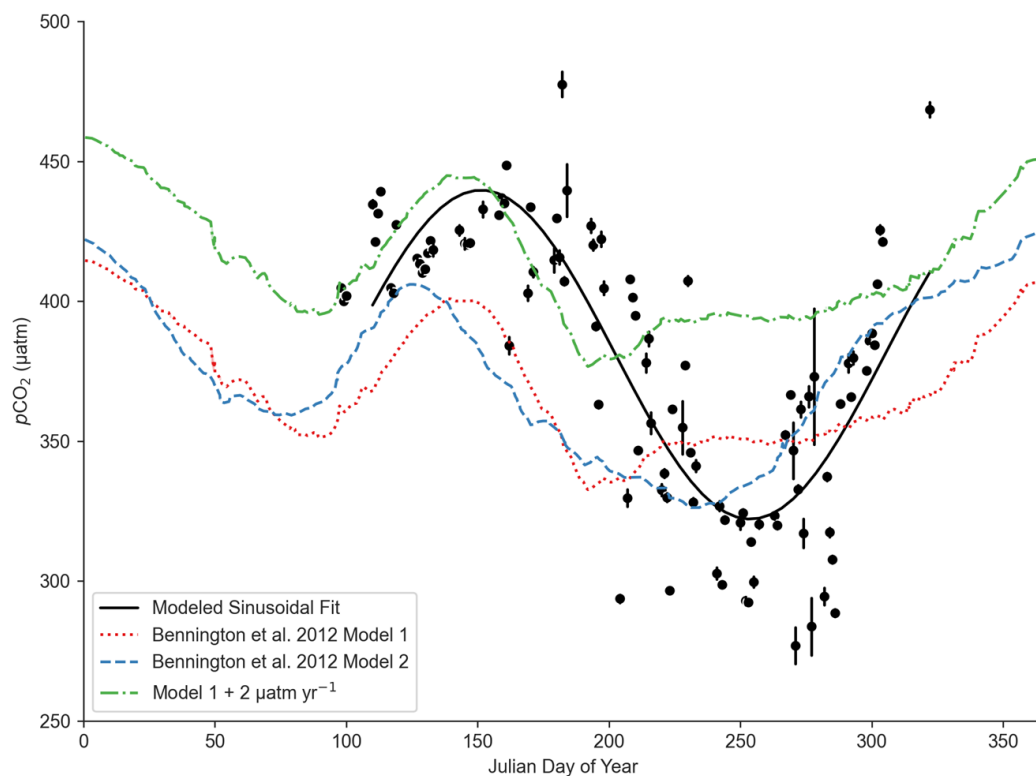330 al., 2020).

331 The pelagic $p\mathrm{CO}_2$ cycle displayed a greater seasonal variability than the simu-
332 lated time series of Bennington et al. (2012) (Figure 4). Annual $p\mathrm{CO}_2$ summer minima
333 and spring maxima were approximately 330 and 400 µatm in Model 1 of that work,
334 compared to 322 and 440 µatm in this study's synthetic annual time series of pelagic
335 observations. Bennington et al. modeled surface water equilibrium with an atmo-
336 spheric $p\mathrm{CO}_2$ of 360 µatm at the end of a mixing period spanning late April-late June
337 1997-2001. At the end of destratification in this (2019-2022) study, a mean surface
338 water $p\mathrm{CO}_2$ of 430 ± 30 µatm (±s.d.) was observed, which was indistinguishable from
339 contemporaneous atmospheric $p\mathrm{CO}_2$. The two models presented by Bennington et
340 al. differed in their treatment of primary production limitation, which resulted in the
341 greatest differences after spring mixing, when this study's observations also displayed
342 high spatial variability.

343 The observed increase in spring mixing period $p\mathrm{CO}_2$ was consistent with the
344 magnitude of atmospheric CO_2 concentration increase (c. 2 ppm yr^{-1}, Keeling and
345 Keeling (2017)) over the 23 years separating the modeled period of Bennington et al.
346 and these observations, as well as the direction of increase in Lake Superior surface
347 water $p\mathrm{CO}_2$ calculated from pH and A_T over the period 1992-2019 by Minor and
348 Brinkley (2022). The precise rate of increase of Lake Superior surface water $p\mathrm{CO}_2$ over
349 decadal timescales remains difficult to constrain, but its continuing near-atmospheric
350 equilibrium state, along with radiocarbon measurements indicating rapid ($<$3 years)
351 recycling of the DIC pool (Zigah et al., 2011), indicates that it mirrors atmospheric
352 $p\mathrm{CO}_2$ during mixing periods and will continue to do so.

353 The magnitude of seasonal variability in Lake Superior $p\mathrm{CO}_2$ was comparable
354 to that of subtropical ocean regions (Bates, 2001), but shifted in the year. In terms
355 of $p\mathrm{CO}_2$ phenology, Lake Superior resembled the Arctic ocean most closely, despite
356 exhibiting a much larger amplitude (Orr et al., 2022). Scarcity of data from November-
357 April prevented great confidence in extrapolation to those periods, but models indicate
358 that Lake Superior $p\mathrm{CO}_2$ likely remains supersaturated or near-atmospheric equilib-
359 rium throughout that period (Bennington et al., 2012). Interannually-variable winter-
360 time ice cover (White et al., 2012) may modify the expected CO_2 efflux.

3.5 Competing Drivers of $p\mathrm{CO}_2$

362 Deconvoluting the pelagic $p\mathrm{CO}_2$ cycle (Figure 3b) into inferred drivers shed light
363 on biogeochemical cycling in Lake Superior. The method of Takahashi et al. (1993) was
364 used to separate measured $p\mathrm{CO}_2$ into thermal ($p\mathrm{CO}_{2\ T}$) and biophysical ($p\mathrm{CO}_{2\ BP}$)

Figure 4. Median daily observations of pelagic surface water $p\mathrm{CO_2}$ observed during 2019-2022 compared with Models 1 and 2 from Bennington et al. (2012), which described mean lake surface $p\mathrm{CO_2}$ 1997-2001. A 46 µatm translation of Model 1 to account for 23 years' atmospheric $\mathrm{CO_2}$ increase (assuming 2 µatm yr^{-1}) aligned spring and mixing season modeled results with contemporary observations.

signals

$$pCO_{2\,T} = \overline{pCO_2} \cdot e^{\left(\frac{\partial ln(pCO_2)}{\partial T}[T-\overline{T}]\right)} \qquad (6)$$

$$pCO_{2\,BP} = pCO_2 \cdot e^{\left(\frac{\partial ln(pCO_2)}{\partial T}[\overline{T}-T]\right)} \qquad (7)$$

Seasonal warming was expected to increase pCO_2 and thus promote CO_2 efflux. The remaining variation was ascribed to biophysical processes including production, respiration, gas flux, and river inputs. $CaCO_3$ dissolution and precipitation were neglected in this analysis of greatly-undersaturated Lake Superior. Overbars indicated arithmetic mean values in the literature source, but this study analyzed an incomplete annual time series of pCO_2, so mean temperature ($\overline{T}$) and mean pCO_2 ($\overline{pCO_2}$) were adjusted to 1 °C and 400 µatm to ensure convergence of the driver signals at the beginning of the observed period. The temperature partial derivative of $ln(pCO_2)$ was calculated via PyCO$_2$SYS, yielding an average value of 0.03606 °C^{-1} for Lake Superior over the temperature range 0-20 °C (code in Supporting Text S2). This temperature dependence is in good agreement with values used in previous studies (0.038 °C^{-1} Atilla et al. (2011); 0.0384 °C^{-1} Lynch et al. (2010)).

Plotting the measured, thermal, and biophysical pCO_2 signals illustrated the interplay of these competing drivers of pCO_2 in Lake Superior (Figure 5). Seasonal temperature effects were visible as the springtime increase and autumn decrease in $pCO_{2\,T}$, opposed by the summertime dip in $pCO_{2\,BP}$. Measured pCO_2 lay suspended between the curves. The degree to which thermal vs. biophysical drivers control pCO_2 can be conceptualized as the vertical distance between the measured curve and its two drivers; in spring, measured pCO_2 was closely tied to $pCO_{2\,T}$, indicating that most of the spring trend in pCO_2 was driven by seasonal warming. pCO_2 moved equidistant between drivers before dipping with the biophysical curve through the summer. Quantitatively, the ratio of thermal to biophysical control of pCO_2 can be calculated (Fassbender et al., 2018; Takahashi et al., 2002) as

$$R_{T\,BP^{-1}} = \frac{\max(pCO_{2\,T}) - \min(pCO_{2\,T})}{\max(pCO_{2\,BP}) - \min(pCO_{2\,BP})} \qquad (8)$$
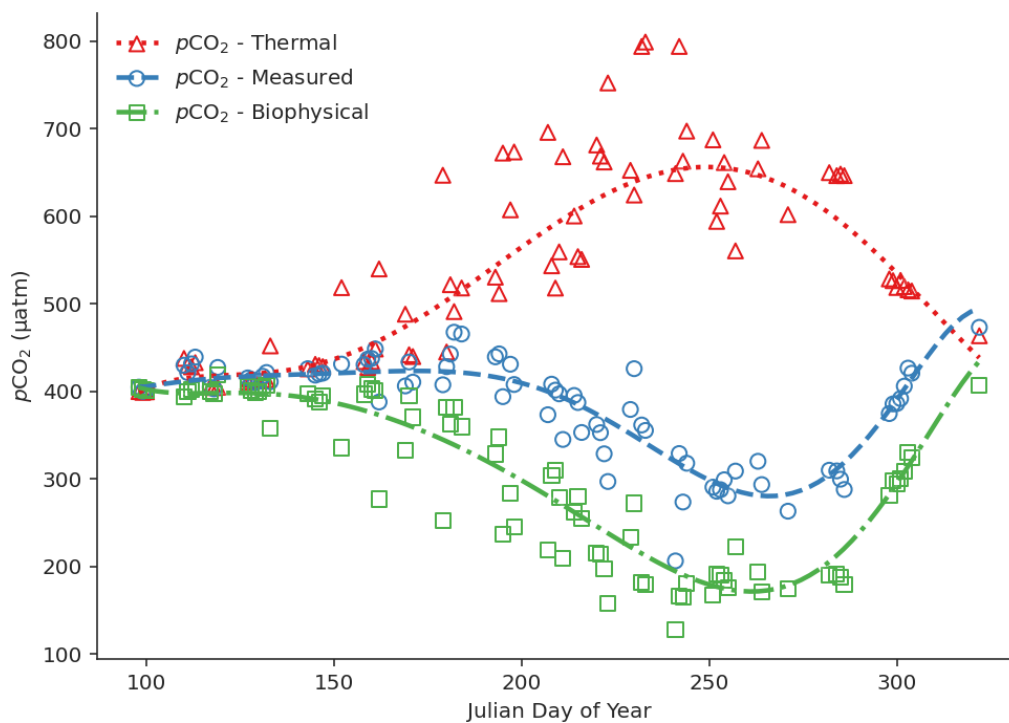
which yielded a value of 1.1 using the regressions in Figure 5, indicating roughly equal thermal and biophysical driver magnitudes over the ice-free period. Interestingly, this value aligns with that of the Atlantic Ocean at the approximate latitude of Lake Superior (Fassbender et al., 2018), which raises questions about latitudinal gradients in $R_{T\,BP^{-1}}$ in inland waters compared to marine systems. Minor et al. (2019) found majority biophysical control of calculated pCO_2 from discrete samples of Lake Superior surface water in 2014-2016, and the degree of dominance varied year-to-year.
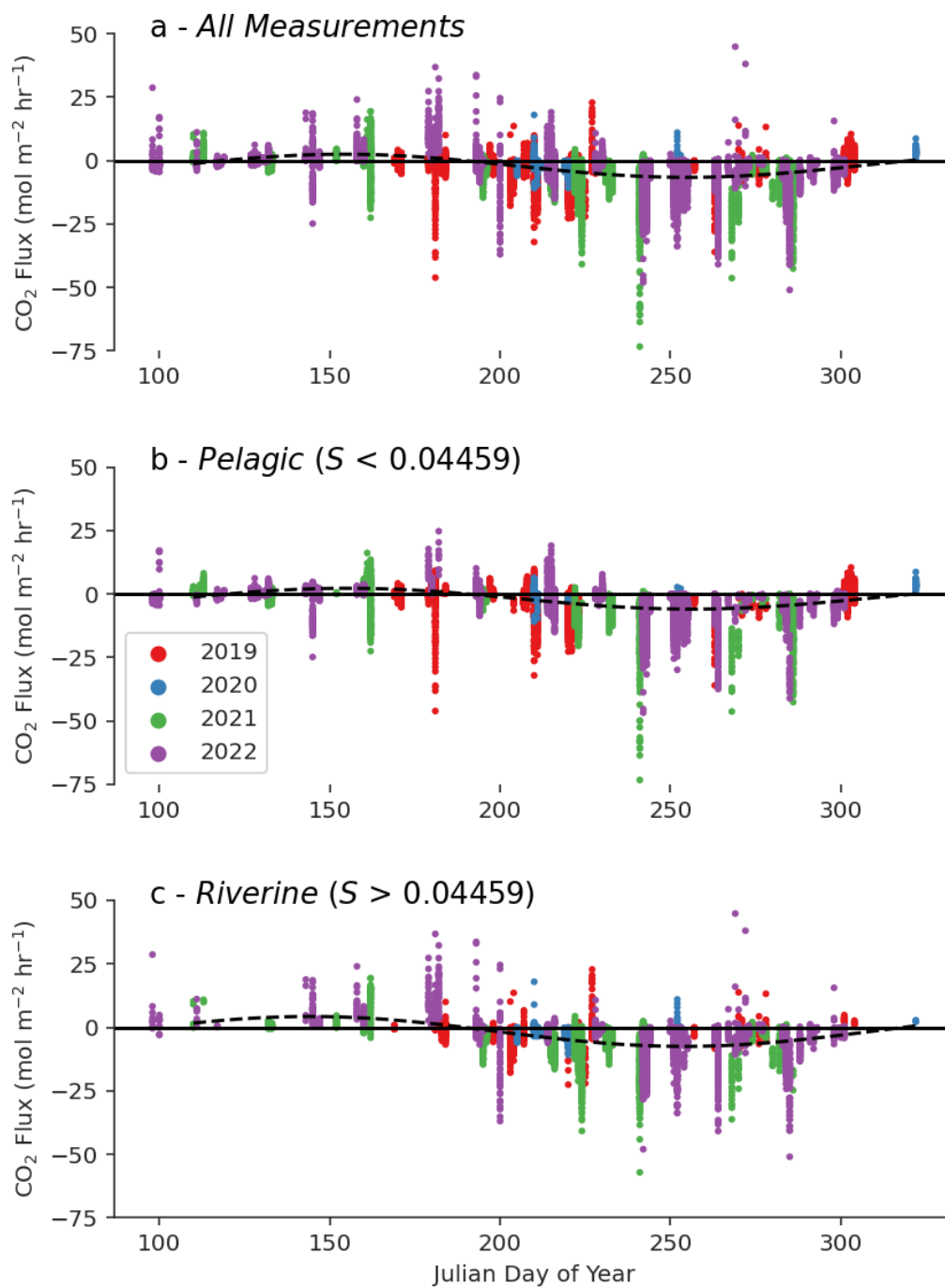
3.6 CO$_2$ Flux Variability

CO$_2$ flux displayed sinusoidal behavior similar to that of pCO_2, but with a greater degree of variability within individual cruises (Figure 6). Sinusoidal regression of observations of CO$_2$ flux (grouped by 0.01° box and date) over Julian day indicated similar seasonality to the pCO_2 annual cycle. For pelagic observations, there was a baseline value of -1.88 mmol m^{-2} d^{-1} (negative values indicating influx) and an amplitude of 4.11 mmol m^{-2} d^{-1}. The most extreme values were observed in mid-summer, when high wind speeds coupled with CO$_2$-undersaturated surface waters to create high instantaneous rates of CO$_2$ drawdown exceeding 70 mmol m^{-2} d^{-1}.

3.7 Competing Drivers of CO$_2$ Flux

This research parameterized CO$_2$ flux from CO$_2$ saturation and wind velocity, so discussion of the drivers of CO$_2$ flux over Lake Superior is limited to the relative

Figure 5. Deconvolution of median daily measured sea surface $p\mathrm{CO_2}$ (circles/dashed line) into Biophysical (squares/dash-dot line) and Thermal (triangles/dotted line) drivers. Septic power function regressions are shown as visual aids, and their equations are given in the Supporting Information.

Figure 6. Parameterized CO_2 flux grouped by $0.01°$ squares and date during transects of Lake Superior for a synthetic annual time series 2019-2022. Black dashed lines represent sinusoidal regressions of each time series.

dominance of these two factors over various timescales. The degree to which either predictor explains flux magnitude can be quantified using linear regression of the absolute value of flux against the absolute values of k or $\Delta p\text{CO}_2$, log-transformed to approach normality. R^2 values then indicate the fraction of variation predicted by each variable: 59.2% of CO_2 flux variability was predicted by k and 43.4% by $\Delta p\text{CO}_2$, indicating that k predicted CO_2 flux better than $\Delta p\text{CO}_2$ in Lake Superior on multiannual timescales. This result also explains some CO_2 flux variability driven by k variability in any given transect visible as departures from the sub-annual cycle in Figure 6. This result contrasted with the conclusions of Natchimuthu et al. (2017) that $\Delta p\text{CO}_2$ variability dominated over k variability over long (days to weeks) periods in small hemiboreal lakes. This may be due to the relatively wider range in $p\text{CO}_2$ observed by Natchimuthu et al. (714-12961 µatm) which overwhelmed k variability, as well as the smaller fetch associated with their sites.
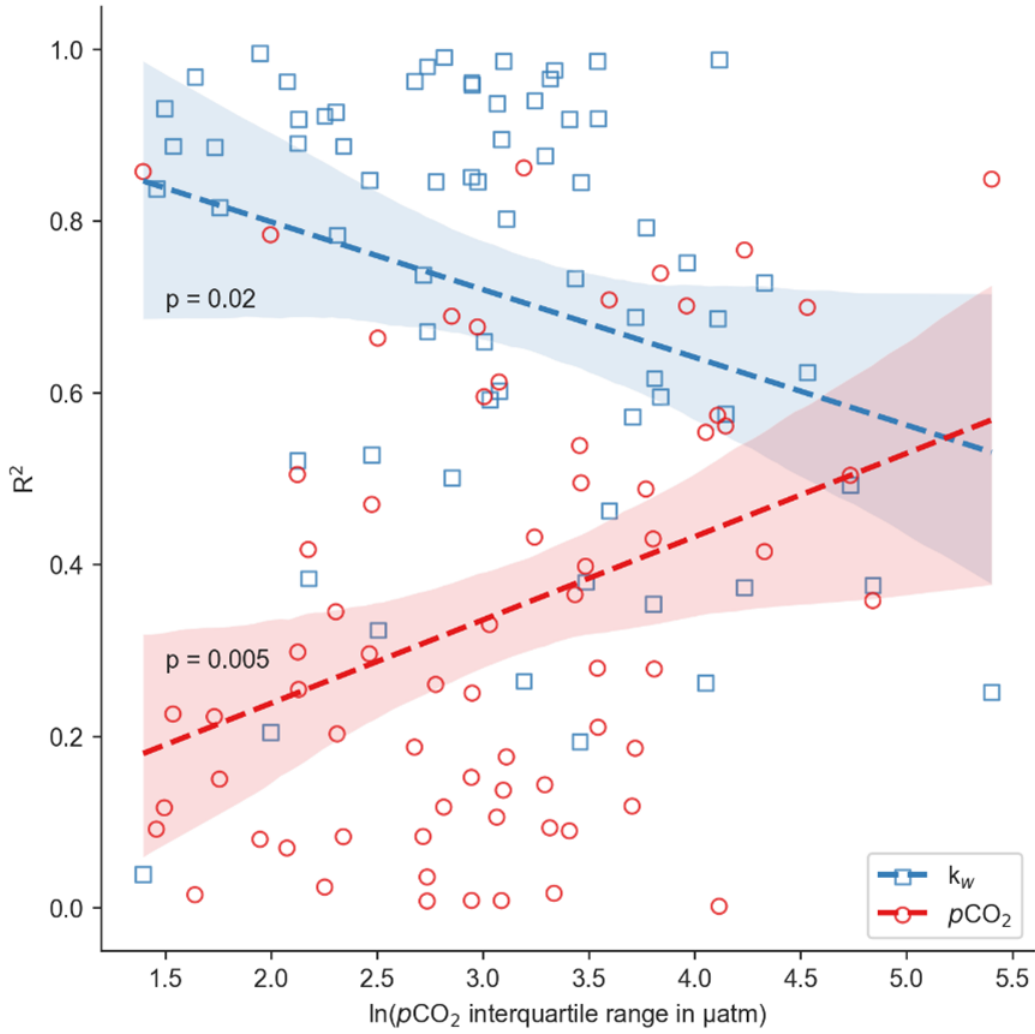
A similar pattern emerged when individual cruises were considered. 52 of 69 cruises demonstrated superior predicting ability of CO_2 flux by k relative to $\Delta p\text{CO}_2$, as quantified by higher R^2 values resulting from a type-I linear regression. The prediction capacity of k diminished in cruises with a high interquartile range of $p\text{CO}_2$. Linear regressions of cruise-level R^2 values over log-transformed $p\text{CO}_2$ interquartile range indicated significant relationships for both k R^2 values (p = 0.02) and $\Delta p\text{CO}_2$ R^2 values (p = 0.005) (Figure 7).

These results illustrate the importance of capturing observations representing a full and continuous distribution of $p\text{CO}_2$ and wind velocities for a study system. The relative importance of k and $\Delta p\text{CO}_2$ depended on their ranges over a timescale of interest, but in a system like Lake Superior with limited variability in $p\text{CO}_2$ (compared to small inland lakes), k dominated CO_2 flux variability across all timescales, demonstrating a crucial difference between this large lake and its smaller peers. Observations and models of CO_2 flux in large lakes miss the full picture if they neglect to fully characterize both $\Delta p\text{CO}_2$ and k, especially in systems where these values exhibit wide distributions.

3.8 Total CO_2 Flux Estimation

Net CO_2 air-sea flux over the observed seasons was obtained via integration of the sinusoidal regressions of instantaneous CO_2 flux (Figure 6) across the observed time domain: Julian day 100 (April 9 or 10) through 300 (November 26 or 27). The resulting values (Table 1) were multiplied by the total area of Lake Superior (8.21 x 10^{10} m^2) to yield total fluxes, but it was not clear what fraction of the lake is considered "pelagic" vs. "riverine". We suggest that these values serve as bounds for the net CO_2 flux of Lake Superior throughout the ice-free season. Uncertainty in integrated fluxes was determined by bootstrap random resampling with replacement of data underlying the sinusoidal regressions of CO_2 flux for 100 repetitions and given as the standard deviation of the repetition net fluxes. .

The resulting CO_2 influx on the order of 30 Gmol C (360 Gg C) was similar in magnitude but opposite in sign to the only fully-annual modeled CO_2 flux: an mean net annual efflux of 16 Gmol C yr^{-1} (190 Gg C yr^{-1}) over the period 1997-2001 (Bennington et al. 2012). The discrepancy is accounted for by winter supersaturation of surface $p\text{CO}_2$. Assuming the veracity and comparability of the above values, an efflux of 46 Gmol C (550 Gg C) during Julian days 301-99 is implied. The rough approximations of carbon budgets allowed by available annual CO_2 fluxes continues to prohibit integration of Lake Superior into regional and global C budgets. There remains the possibility that the modeled annual CO_2 flux and this study's observed sub-annual flux are not comparable due to two intervening decades of ecological and climate change, an under-constrained modeled $p\text{CO}_2$ cycle, and ongoing uncertainty about comparisons

Figure 7. Cruise-level R^2 values for the prediction of CO_2 flux by k (gas transfer velocity) and $\Delta p CO_2$, separated by interquartile ranges of the distribution of $p CO_2$ observed in each cruise. Shaded intervals around type-I linear regressions indicate 95% confidence intervals. Larger interquartile ranges of $p CO_2$ within cruises are associated with poorer prediction of CO_2 flux by k relative to $\Delta p CO_2$. Type-I linear regressions indicate significant slopes (indicated by p-values) for n = 69 cruises.

Table 1. Time-integrated fluxes of CO_2 over the air-water interface of Lake Superior ascribed to Pelagic and Riverine chemical regimes for Julian Days 100-300. Uncertainties are given as standard deviations propagated via bootstrap resampling with replacement for 100 repetitions. Negative signs indicate influx.

Region	CO_2 Areal Flux (mol C m^{-2})	CO_2 Total Flux (Gmol C)
Pelagic	-0.3744 ± 0.0068	-30.78 ± 0.56
Riverine	-0.324 ± 0.023	-26.5 ± 1.9

of measured versus calculated $p\mathrm{CO}_2$ in Lake Superior. An updated observation-based and/or process model constrained by spatially- and temporally- comprehensive direct observations of $p\mathrm{CO}_2$ and CO_2 flux is required for substantive comparisons of observed and modeled C cycling.

A rough estimate of net community production (NCP) can be inferred from the net CO_2 air-sea flux and the calculated DIC time series as

$$\mathrm{NCP} = \int_{t=100}^{300} \left(\frac{\delta \mathrm{DIC}}{\delta t} \cdot \mathrm{MLD}_t - \mathrm{CO}_2 \ \mathrm{Flux} \right) \tag{9}$$

Assuming a constant MLD of 20 m (Bennington et al., 2010), a surface DIC drawdown (Figure 2d) around 10 µmol kg^{-1} between Julian days 100-300, and a CO_2 air-sea flux of 30 Gmol C yields an NCP of 46 Gmol C for the observed period. Spatial variability of MLD and weaker thermal structure before summer stratification likely makes this an underestimate and biases this estimate of NCP. Our estimated ice-free season surface water NCP is more than 200x smaller than the 9.73 Tg y^{-1} whole-lake annual primary production reported by Sterner (2010), in agreement with previous inferences of high organic C turnover rates in Lake Superior (N. R. Urban, 2005). Future studies should establish an annual NCP to compare with previously-reported values (e.g. N. R. Urban, 2005) which don't constrain the sign of NCP.

4 Discussion

Four years of surface $p\mathrm{CO}_2$ measurements gathered on transects across Lake Superior were used to elucidate inorganic carbon system variability across temporal and spatial scales. Ice-free season (April-November) observations yielded a detailed account of the seasonal $p\mathrm{CO}_2$ cycle, driven by thermal and biophysical drivers acting in opposition to perturb surface $p\mathrm{CO}_2$ from its interannual baseline state of atmospheric equilibrium, resulting in sustained periods of CO_2 influx and efflux. Spatial variability in the inorganic C system effected by riverine influence was highlighted by separating the lake into pelagic and riverine regimes. Integration of instantaneous CO_2 fluxes over the ice-free period resulted in April-November CO_2 influxes of 32.80 ± 0.61 Gmol C (pelagic) and 26.5 ± 2.1 Gmol C (riverine), which are considered bounding values for the whole-lake mean CO_2 flux during observed periods of 2019-2022; annual net CO_2 flux remains uncertain. These results point towards a significant role of Lake Superior to interact with global and regional C cycling and climate change. Increases in surface $p\mathrm{CO}_2$ over the last two decades illustrate that Lake Superior is undergoing CO_2 invasion in agreement with Phillips et al. (2015). Variability in CO_2 flux, parameterized by $\Delta p\mathrm{CO}_2$ and gas transfer velocity k, was dominated by k over all time scales, though this effect diminished over periods of larger spatial variability in $p\mathrm{CO}_2$.

A paucity of early Spring and late Fall data hindered analysis of periods at the extremes of the ice-free season, which could shed light on the effects of ice-off as a driver of CO_2 flux (cf. Ahmed et al., 2019). As previously noted, there may be some bias in wind-parameterized gas transfer velocities associated with dual-tracer experiments (Yang et al., 2022), such that the gas transfer velocities calculated here may be underestimates by as much as 20%. Future studies should seek to explore wind speed gas flux parameterization applications in large lakes.

4.1 Consequences of Increasing $p\mathrm{CO}_2$

Among the most impactful findings of this research is the observation that Lake Superior surface $p\mathrm{CO}_2$ maintains near-equilibrium with the overlying atmosphere over multi-year periods. Temperature variability and biogeochemical processes drive sea-

sonal departures of $p\text{CO}_2$ from atmospheric equilibrium (effecting the expected net annual CO_2 efflux), yet surface water $p\text{CO}_2$ returns to a baseline state of atmospheric equilibrium on timescales shorter than a year. This fact has several significant consequences in a world of increasing atmospheric CO_2 concentration:

First, the solubility pump of Lake Superior acts as a partial CO_2 sink which can be approximated by an equilibrium calculation: Assuming A_T = 840 μmol kg^{-1}, T = 3.98 °C (temperature of maximum density during destratification), an initial $p\text{CO}_2$ = 400 µatm, and an atmospheric $\Delta p\text{CO}_2$ Δt^{-1} = 2.50 µatm yr^{-1}, then a CO2SYS calculation indicates ΔDIC Δt^{-1} = 0.184 µmol kg^{-1} yr^{-1}, which is multiplied by the approximate mass of Lake Superior (1.21 x 10^{17} kg) to give a CO_2 storage of 22.3 Gmol C yr^{-1} (267 Gg C yr^{-1}) due to increasing atmospheric CO_2 alone. This storage is characteristic of any body of water maintaining CO_2 equilibrium with a non-steady-state atmosphere. It acts alongside C sources (e.g. DIC loading) and sinks (e.g. C burial) to compose the net annual C budget of Lake Superior. Development of an annual net CO_2 flux using expanded observational and modeling capabilities may yield insights on all of these contributors. If atmospheric $p\text{CO}_2$ were stable, then Superior's annual net CO_2 efflux could be larger than it is today, mirroring the case of the pre-industrial global ocean, which likely acted as a CO_2 source instead of a sink (Cartapanis et al., 2018).

Second, Lake Superior's water chemistry will undergo changes as a result of consistently-higher $p\text{CO}_2$. Its weak CO_2 buffer (Revelle factor 25-30 in calculations in this work, compared to marine values 8-16 (Sarmiento & Gruber, 2006)) and absence of sediment carbonate buffer (unlike neighboring Lake Michigan) result in relatively high sensitivity to atmospheric CO_2 acidification. The outcomes of hypothesized lake acidification mirror those in the ocean: decreasing pH and CaCO_3 saturation states, impacts on primary producer communities, changes to metal ion activities, and other phenomena with potentially detrimental ecosystem effects (Doney et al., 2009). Trends in A_T and temperature may modify the speciation (e.g. $[\text{CO}_3^{2-}]$, pH) of the inorganic carbon system as well as the seasonal and spatial expression of the surface water $p\text{CO}_2$ cycle, but not the surface $p\text{CO}_2$ of a system at equilibrium with the atmosphere.

Third, efforts to observe Lake Superior's inorganic C system must capture a greater fraction of the annual cycle and spatial variability to constrain these changes. The twice-annual time series of chemical parameters (including glass electrode pH and Gran titration alkalinity) collected by US EPA Great Lakes National Program Office includes samples over a broad spatial scale, during periods of mean CO_2 efflux (April-May) and influx (August-September) but fails to observe intervening periods which provide context for interannual variability of the annual $p\text{CO}_2$ cycle. Undersampling a complex signal like inorganic C chemistry delays detection of climate change effects (Carter et al., 2019). A more complete picture of biogeochemical parameters is sorely needed during the current period of climate change and ecological disruption. This gap in observational capabilities can be addressed by a sustained campaign of higher-quality, higher-frequency measurements of inorganic C parameters in the Laurentian Great Lakes.

4.2 Observational Challenges and Opportunities

Environmental and instrumental challenges limit deployment of underway $p\text{CO}_2$ systems as tools for biogeochemical observation on large lakes like Superior. These instruments describe only a small fraction of a water body at any given time, which complicates efforts to generalize results to the system as a whole. A network of similar sensors equipped on moorings, vessels of opportunity, and other vehicles (drifters, saildrones, wavegliders) may be suited for more synoptic observation. Seasonal ice cover limits winter deployment of autonomous sensors, and has long acted as a blinder

focusing scientific attention on more accessible seasons. Novel observation platforms designed to observe under-ice $p\text{CO}_2$ (M. D. DeGrandpre et al., 2019; Lee et al., 2022) demonstrate the potential to expand the horizons of inorganic C observation in seasonally ice-covered lakes. Direct measurements of gas flux may also be obtained by eddy covariance towers in the vicinity of the Great Lakes (Shao et al., 2015).

This research grappled with problems of bias in transect data due to overrepresentation of certain regions in space (the far western lake) and time (summer). Although these problems were partially addressed by regression analysis and separation of pelagic and riverine regimes, future work should consider other drivers of spatial and temporal heterogeneity, for example: dissolved organic matter and chlorophyll measured by in-situ instruments or remote sensing (e.g. Lohrenz et al., 2018; Sims et al., 2023). Expanded monitoring of $p\text{CO}_2$ and related chemical properties in the Laurentian Great Lakes provides a fruitful avenue for observation and modeling of CO_2 budgets in the world's largest surface freshwater resource.

4.3 Conclusions

This study provided the most comprehensive observations to date of surface $p\text{CO}_2$ variability in Earth's largest freshwater lake by area and demonstrated techniques for inferring C cycling drivers in an understudied system. As the present perturbation of Earth's C cycle continues, the need for such knowledge to inform water and climate policy will grow apace, requiring continuing innovation of observational and modeling capabilities. This is as true for the Laurentian Great Lakes as for the African Rift Lakes and other understudied surface waters of the world.

A spatially-comprehensive, fully annual CO_2 flux budget is not achievable with the data presented here because of spatial and temporal gaps in the time series presented. Future work must perform more observation of neglected regions in space and time, extrapolation to unobserved domains, and generalization of observed fluxes and drivers by modeling efforts. To this end, we recommend further development of observational strategies such as underway data collection, moored and autonomous instrumentation, remote sensing, and winter limnology techniques to better constrain CO_2 flux in Superior and other large lake systems. Efforts to resolve the modeled C budgets of the Great Lakes will benefit from a greater number of CO_2 measurements to constrain and correct models (cf. Gloege et al., 2022). Insights into the balance of productivity and respiration may result from pairing a large $p\text{CO}_2$ survey with measurements of other biogeochemical tracers such as dissolved oxygen (Evans et al., 2022) or primary productivity (Sterner, 2010). As ice cover of temperate lakes declines with climate change, the period amenable to transects of seasonally ice-covered lakes will grow. This disappearance of the ice cover regime is among driving forces of the sub-discipline of winter limnology, which studies a vanishing environment (Ozersky et al., 2021). It is unclear how changes in ice cover will affect annual $p\text{CO}_2$ fluxes in these changing lakes systems. Spatially- and temporally- comprehensive observations of element cycling in these large lakes hint at the depth and complexity of biogeochemical functions responding and feeding back to a changing planet.

Open Research Section

Underway data generated by transects of the *RV Blue Heron* is freely available at its Rolling Deck to Repository site: *https://www.rvdata.us/search/vessel/Blue%20Heron*.

References

Ahmed, M., Else, B. G. T., Burgers, T. M., & Papakyriakou, T. (2019, March). Variability of surface water pCO_2 in the Canadian Arctic Archipelago from 2010 to 2016. *J. Geophys. Res. Oceans*, *124*(3), 1876–1896. doi: 10.1029/2018JC014639

Alin, S. R., & Johnson, T. C. (2007, September). Carbon cycling in large lakes of the world: A synthesis of production, burial, and lake-atmosphere exchange estimates. *Global Biogeochem. Cycles*, *21*(GB3002). doi: 10.1029/2006GB002881

Atilla, N., McKinley, G. A., Bennington, V., Baehr, M., Urban, N., DeGrandpre, M., ... Wu, C. (2011, May). Observed variability of Lake Superior pCO₂. *Limnol. Oceanogr.*, *56*(3), 775–786. doi: 10.4319/lo.2011.56.3.0775

Austin, J., & Colman, S. (2008, November). A century of temperature variability in Lake Superior. *Limnol. Oceanogr.*, *53*(6), 2724–2730. doi: 10.4319/lo.2008.53.6.2724

Austin, J., Hill, C., Fredrickson, J., Weber, G., & Weiss, K. (2022, September). Characterizing temporal and spatial scales of radiatively driven convection in a deep, ice-free lake. *Limnol. Oceanogr.*, lno.12203. doi: 10.1002/lno.12203

Bates, N. R. (2001, January). Interannual variability of oceanic CO2 and biogeochemical properties in the Western North Atlantic subtropical gyre. *Deep Sea Res. Part II Top. Stud. Oceanogr.*, *48*(8-9), 1507–1528. doi: 10.1016/S0967-0645(00)00151-X

Bennington, V., McKinley, G. A., Kimura, N., & Wu, C. H. (2010, December). General circulation of Lake Superior: Mean, variability, and trends from 1979 to 2006. *J. Geophys. Res.*, *115*(C12), C12015. doi: 10.1029/2010JC006261

Bennington, V., McKinley, G. A., Urban, N. R., & McDonald, C. P. (2012, September). Can spatial heterogeneity explain the perceived imbalance in Lake Superior's carbon budget? *J. Geophys. Res.*, *117*(G03020). doi: 10.1029/2011JG001895

Broecker, W. S., & Peng, T.-H. (1982). *Tracers in the Sea*. Lamont-Doherty Earth Observatory, Columbia University.

Bushinsky, S. M., Takeshita, Y., & Williams, N. L. (2019, September). Observing changes in ocean carbonate chemistry: Our autonomous future. *Curr. Clim. Change Rep.*, *5*(3), 207–220. doi: 10.1007/s40641-019-00129-8

Cartapanis, O., Galbraith, E. D., Bianchi, D., & Jaccard, S. L. (2018, November). Carbon burial in deep-sea sediment and implications for oceanic inventories of carbon and alkalinity over the last glacial cycle. *Clim. Past*, *14*(11), 1819–1850. doi: 10.5194/cp-14-1819-2018

Carter, B. R., Williams, N. L., Evans, W., Fassbender, A. J., Barbero, L., Hauri, C., ... Sutton, A. J. (2019, April). Time of detection as a metric for prioritizing between climate observation quality, frequency, and duration. *Geophys. Res. Lett.*, *46*(7), 3853–3861. doi: 10.1029/2018GL080773

Cavallaro, N., Shrestha, G., Birdsey, R., Mayes, M. A., Najjar, R. G., Reed, S. C., ... Zhu, Z. (2018). *Second state of the carbon cycle report* (Tech. Rep.). U.S. Global Change Research Program. doi: 10.7930/Soccr2.2018

Chapra, S. C., Dove, A., & Warren, G. J. (2012, September). Long-term trends of Great Lakes major ion chemistry. *J. Great Lakes Res.*, *38*(3), 550–560. doi: 10

.1016/j.jglr.2012.06.010

Cole, J. J. (2013). *Freshwater ecosystems and the carbon cycle* (No. 18). Olden-dorf/Luhe Germany: International Ecology Institute.

Cole, J. J., & Caraco, N. F. (1998, June). Atmospheric exchange of carbon dioxide in a low-wind oligotrophic lake measured by the addition of SF_6. *Limnol. Oceanogr.*, *43*(4), 647–656. doi: 10.4319/lo.1998.43.4.0647

Cole, J. J., Caraco, N. F., Kling, G. W., & Kratz, T. K. (1994, September). Carbon Dioxide Supersaturation in the Surface Waters of Lakes. *Science*, *265*(5178), 1568–1570. doi: 10.1126/science.265.5178.1568

DeGrandpre, M., Evans, W., Timmermans, M.-L., Krishfield, R., Williams, B., & Steele, M. (2020, June). Changes in the Arctic Ocean Carbon Cycle With Diminishing Ice Cover. *Geophys. Res. Lett.*, *47*(12). doi: 10.1029/2020GL088051

DeGrandpre, M. D., Lai, C.-Z., Timmermans, M.-L., Krishfield, R. A., Proshutinsky, A., & Torres, D. (2019, June). Inorganic carbon and pCO_2 variability during ice formation in the Beaufort Gyre of the Canada Basin. *J. Geophys. Res. Oceans*, *124*(6), 4017–4028. doi: 10.1029/2019JC015109

Desai, A. (2022). *AmeriFlux BASE US-PFa Park Falls/WLEF*. AmeriFlux AMP. doi: 10.17190/AMF/1246090

Desai, A. R., Austin, J. A., Bennington, V., & McKinley, G. A. (2009, December). Stronger winds over a large lake in response to weakening air-to-lake temperature gradient. *Nature Geosci*, *2*(12), 855–858. doi: 10.1038/ngeo693

Dickson, A. G., Sabine, C. L., Christian, J. R., Bargeron, C. P., & Organization, N. P. M. S. (Eds.). (2007). *Guide to best practices for ocean CO_2 measurements* (No. 3). Sidney, BC: North Pacific Marine Science Organization.

Doney, S. C., Fabry, V. J., Feely, R. A., & Kleypas, J. A. (2009, January). Ocean acidification: The other CO_2 problem. *Annu. Rev. Mar. Sci.*, *1*(1), 169–192. doi: 10.1146/annurev.marine.010908.163834

Evans, W., Lebon, G. T., Harrington, C. D., Takeshita, Y., & Bidlack, A. (2022, March). Marine CO_2 system variability along the northeast Pacific Inside Passage determined from an Alaskan ferry. *Biogeosciences*, *19*(4), 1277–1301. doi: 10.5194/bg-19-1277-2022

Fassbender, A. J., Rodgers, K. B., Palevsky, H. I., & Sabine, C. L. (2018, October). Seasonal asymmetry in the evolution of surface ocean pCO_2 and pH thermodynamic drivers and the influence on Sea-Air CO_2 flux. *Global Biogeochem. Cycles*, *32*(10), 1476–1497. doi: 10.1029/2017GB005855

Feely, R., Sabine, C., Takahashi, T., & Wanninkhof, R. (2001). Uptake and storage of carbon dioxide in the ocean: The global CO_2 survey. *Oceanog*, *14*(4), 18–32. doi: 10.5670/oceanog.2001.03

Firing, E., Filipe, Barna, A., & Abernathey, R. (2021, March). *TEOS-10/GSW-Python: V3.4.1*. Zenodo. doi: 10.5281/zenodo.4631364

Fuller, K., & Shear, H. (Eds.). (1995). *The Great Lakes: An environmental atlas and resource book* (3rd ed.). Chicago, Ill. : Toronto, Ont: Great Lakes National Program Office, U.S. Environmental Protection Agency ; Government of Canada.

Gloege, L., Yan, M., Zheng, T., & McKinley, G. A. (2022, February). Improved quantification of ocean carbon uptake by using machine learning to merge global models and pCO_2 data. *J. Adv. Model Earth Syst.*, *14*(2). doi: 10.1029/2021MS002620

Harris, C. R., Millman, K. J., van der Walt, S. J., Gommers, R., Virtanen, P., Cournapeau, D., . . . Oliphant, T. E. (2020, September). Array programming with NumPy. *Nature*, *585*(7825), 357–362. doi: 10.1038/s41586-020-2649-2

Hill, K., Dauphinee, T., & Woods, D. (1986). The extension of the Practical Salinity Scale 1978 to low salinities. *IEEE J. Ocean. Eng.*, *11*(1), 109–112. doi: 10.1109/JOE.1986.1145154

Ho, D. T., Law, C. S., Smith, M. J., Schlosser, P., Harvey, M., & Hill, P.   (2006).   Measurements of air-sea gas exchange at high wind speeds in the Southern Ocean: Implications for global parameterizations. *Geophys. Res. Lett.*, *33*(16), L16611. doi: 10.1029/2006GL026817

Humphreys, M. P., Sandborn, D. E., Gregor, L., Pierrot, D., van Heuven, S., S.M.A.C., . . . Wallace, D.   (2020).   PyCO2SYS: Marine carbonate system calculations in Python. *Zenodo*. doi: 10.5281/zenodo.3744275

Hunter, J. D. (2007). Matplotlib: A 2D Graphics Environment. *Comput. Sci. Eng.*, *9*(3), 90–95. doi: 10.1109/MCSE.2007.55

Keeling, R. F., & Keeling, C. D.   (2017).   *Atmospheric monthly in situ CO_2 data - Mauna Loa Observatory, Hawaii.*   UC San Diego Library Digital Collections. doi: 10.6075/J08W3BHW

Lee, C., DeGrandpre, M., Guthrie, J., Hill, V., Kwok, R., Morison, J., . . . Wilkinson, J.   (2022).   Emerging technologies and approaches for in situ, autonomous observing in the Arctic.   *Oceanog.*, *35*(3-4), 210–221.   doi: 10.5670/oceanog.2022.127

Le Quéré, C., Andres, R. J., Boden, T., Conway, T., Houghton, R. A., House, J. I., . . . Zeng, N. (2013, May). The global carbon budget 1959–2011. *Earth Syst. Sci. Data*, *5*(1), 165–185. doi: 10.5194/essd-5-165-2013

Liu, S., Butman, D. E., & Raymond, P. A.   (2020, October).   Evaluating CO_2 calculation error from organic alkalinity and pH measurement error in low ionic strength freshwaters.   *Limnol. Oceanogr. Methods*, *18*(10), 606–622.   doi: 10.1002/lom3.10388

Lohrenz, S., Cai, W.-J., Chakraborty, S., Huang, W.-J., Guo, X., He, R., . . . Tian, H.   (2018, March).   Satellite estimation of coastal pCO_2 and air-sea flux of carbon dioxide in the northern Gulf of Mexico.   *Remote. Sens. Environ.*, *207*, 71–83. doi: 10.1016/j.rse.2017.12.039

Lynch, J. K., Beatty, C. M., Seidel, M. P., Jungst, L. J., & DeGrandpre, M. D. (2010, August).   Controls of riverine CO_2 over an annual cycle determined using direct, high temporal resolution pCO_2 measurements.   *J. Geophys. Res.*, *115*(G3), G03016. doi: 10.1029/2009JG001132

Ma, J., Shu, H., Yang, B., Byrne, R. H., & Yuan, D. (2019, November). Spectrophotometric determination of pH and carbonate ion concentrations in seawater: Choices, constraints and consequences.   *Analytica Chimica Acta*, *1081*, 18–31. doi: 10.1016/j.aca.2019.06.024

McDonald, C. P., Stets, E. G., Striegl, R. G., & Butman, D. (2013, June). Inorganic carbon loading as a primary driver of dissolved carbon dioxide concentrations in the lakes and reservoirs of the contiguous United States. *Global Biogeochem. Cycles*, *27*(2), 285–295. doi: 10.1002/gbc.20032

Minor, E. C., & Brinkley, G.   (2022, January).   Alkalinity, pH, and pCO_2 in the Laurentian Great Lakes: An initial view of seasonal and inter-annual trends. *J. Great Lakes Res.*, S0380133022000211. doi: 10.1016/j.jglr.2022.01.005

Minor, E. C., Forsman, B., & Guildford, S. J.   (2014, June).   The effect of a flood pulse on the water column of western Lake Superior, USA.   *J. Great Lakes Res.*, *40*(2), 455–462. doi: 10.1016/j.jglr.2014.03.015

Minor, E. C., & Oyler, A. R.   (2021, January).   Dissolved organic matter in large lakes: A key but understudied component of the carbon cycle.   *Biogeochemistry*. doi: 10.1007/s10533-020-00733-z

Natchimuthu, S., Sundgren, I., Gålfalk, M., Klemedtsson, L., & Bastviken, D. (2017, January).   Spatiotemporal variability of lake pCO_2 and CO_2 fluxes in a hemiboreal catchment.   *J. Geophys. Res. Biogeosci.*, *122*(1), 30–49.   doi: 10.1002/ 2016JG003449

Oh, N.-H., & Richter, D. D. (2004, November). Soil acidification induced by elevated atmospheric CO_2.   *Global Change Biology*, *10*(11), 1936–1946.   doi: 10.1111/j .1365-2486.2004.00864.x

Orr, J. C., Kwiatkowski, L., & Pörtner, H.-O. (2022, October). Arctic Ocean annual high in $p\mathrm{CO_2}$ could shift from winter to summer. *Nature*, *610*(7930), 94–100. doi: 10.1038/s41586-022-05205-y

Ozersky, T., Bramburger, A. J., Elgin, A. K., Vanderploeg, H. A., Wang, J., Austin, J. A., . . . Zastepa, A. (2021, June). The changing face of winter: Lessons and questions from the Laurentian Great Lakes. *J. Geophys. Res. Biogeosci.*, *126*(6). doi: 10.1029/2021JG006247

Perolo, P., Fernández Castro, B., Escoffier, N., Lambert, T., Bouffard, D., & Perga, M.-E. (2021, November). Accounting for surface waves improves gas flux estimation at high wind speed in a large lake. *Earth Syst. Dynam.*, *12*(4), 1169–1189. doi: 10.5194/esd-12-1169-2021

Phillips, J., McKinley, G., Bennington, V., Bootsma, H., Pilcher, D., Sterner, R., & Urban, N. (2015, June). The potential for $\mathrm{CO_2}$-induced acidification in freshwater: A Great Lakes case study. *Oceanog.*, *25*(2), 136–145. doi: 10.5670/oceanog.2015.37

Podgrajsek, E., Sahlée, E., Bastviken, D., Holst, J., Lindroth, A., Tranvik, L., & Rutgersson, A. (2014, August). Comparison of floating chamber and eddy covariance measurements of lake greenhouse gas fluxes. *Biogeosciences*, *11*(15), 4225–4233. doi: 10.5194/bg-11-4225-2014

Raymond, P. A., & Hamilton, S. K. (2018, June). Anthropogenic influences on riverine fluxes of dissolved inorganic carbon to the oceans: Riverine fluxes of inorganic carbon to the oceans. *Limnol. Oceanogr.*, *3*(3), 143–155. doi: 10.1002/lol2.10069

Reback, J., Jbrockmendel, McKinney, W., Van Den Bossche, J., Augspurger, T., Cloud, P., . . . Seabold, S. (2022, February). *Pandas-dev/pandas: Pandas 1.4.1.* Zenodo. doi: 10.5281/ZENODO.3509134

Sandborn, D. E., Minor, E. C., & Hill, C. (2023, June). Total alkalinity measurement using an open-source platform. *Limnol. Oceanogr. Methods*, *21*(6), 334–344. doi: 10.1002/lom3.10549

Sarmiento, J. L., & Gruber, N. (2006). *Ocean biogeochemical dynamics.* Princeton: Princeton University Press.

Schilder, J., Bastviken, D., van Hardenbroek, M., Kankaala, P., Rinta, P., Stötter, T., & Heiri, O. (2013, November). Spatial heterogeneity and lake morphology affect diffusive greenhouse gas emission estimates of lakes. *Geophys. Res. Lett.*, *40*(21), 5752–5756. doi: 10.1002/2013GL057669

Seabold, S., & Perktold, J. (2010). Statsmodels: Econometric and statistical modeling with Python. In *9th Python in Science Conference.*

Shao, C., Chen, J., Stepien, C. A., Chu, H., Ouyang, Z., Bridgeman, T. B., . . . John, R. (2015, August). Diurnal to annual changes in latent, sensible heat, and $\mathrm{CO_2}$ fluxes over a Laurentian Great Lake: A case study in Western Lake Erie. *J. Geophys. Res. Biogeosci.*, *120*(8), 1587–1604. doi: 10.1002/2015JG003025

Sims, R. P., Ahmed, M. M. M., Butterworth, B. J., Duke, P. J., Gonski, S. F., Jones, S. F., . . . Else, B. G. T. (2023, June). High interannual surface $p\mathrm{CO_2}$ variability in the southern Canadian Arctic Archipelago's Kitikmeot Sea. *Ocean Sci.*, *19*(3), 837–856. doi: 10.5194/os-19-837-2023

Sterner, R. W. (2010, March). In situ-measured primary production in Lake Superior. *J. Great Lakes Res.*, *36*(1), 139–149. doi: 10.1016/j.jglr.2009.12.007

Sterner, R. W. (2021, May). The Laurentian Great Lakes: A biogeochemical test bed. *Annu. Rev. Earth Planet. Sci.*, *49*(1). doi: 10.1146/annurev-earth-071420-051746

Sterner, R. W., Ostrom, P., Ostrom, N. E., Klump, J. V., Steinman, A. D., Dreelin, E. A., . . . Fisk, A. T. (2017, November). Grand challenges for research in the Laurentian Great Lakes. *Limnol. Oceanogr.*, *62*(6), 2510–2523. doi: 10.1002/lno.10585

Sterner, R. W., Reinl, K. L., Lafrancois, B. M., Brovold, S., & Miller, T. R. (2020, December). A first assessment of cyanobacterial blooms in oligotrophic Lake Superior. *Limnol Oceanogr*, *65*(12), 2984–2998. doi: 10.1002/lno.11569

Takahashi, T., Olafsson, J., Goddard, J. G., Chipman, D. W., & Sutherland, S. C. (1993, December). Seasonal variation of CO_2 and nutrients in the high-latitude surface oceans: A comparative study. *Global Biogeochem. Cycles*, *7*(4), 843–878. doi: 10.1029/93GB02263

Takahashi, T., Sutherland, S. C., Sweeney, C., Poisson, A., Metzl, N., Tilbrook, B., ... Nojiri, Y. (2002, January). Global sea–air CO_2 flux based on climatological surface ocean pCO_2, and seasonal biological and temperature effects. *Deep Sea Res. Part II Top. Stud. Oceanogr.*, *49*(9-10), 1601–1622. doi: 10.1016/S0967-0645(02)00003-6

Takahashi, T., Sutherland, S. C., Wanninkhof, R., Sweeney, C., Feely, R. A., Chipman, D. W., ... de Baar, H. J. (2009, April). Climatological mean and decadal change in surface ocean pCO_2, and net sea–air CO_2 flux over the global oceans. *Deep Sea Res. Part II Top. Stud. Oceanogr.*, *56*(8-10), 554–577. doi: 10.1016/j.dsr2.2008.12.009

Takeshita, Y., Johnson, K. S., Martz, T. R., Plant, J. N., & Sarmiento, J. L. (2018, June). Assessment of autonomous pH measurements for determining surface seawater partial pressure of CO_2. *J. Geophys. Res. Oceans*, *123*(6), 4003–4013. doi: 10.1029/2017JC013387

Urban, N., & Desai, A. (2009, January). Are the Great Lakes a significant net source or sink of CO_2? *SIL Proceedings, 1922-2010*, *30*(8), 1283–1288. doi: 10.1080/03680770.2009.11923931

Urban, N. R. (2005). Carbon cycling in Lake Superior. *J. Geophys. Res.*, *110*(C6), C06S90. doi: 10.1029/2003JC002230

Virtanen, P., Gommers, R., Oliphant, T. E., Haberland, M., Reddy, T., Cournapeau, D., ... Vázquez-Baeza, Y. (2020, March). SciPy 1.0: Fundamental algorithms for scientific computing in Python. *Nat Methods*, *17*(3), 261–272. doi: 10.1038/s41592-019-0686-2

Wanninkhof, R. (1992). Relationship between wind speed and gas exchange over the ocean. *J. Geophys. Res.*, *97*(C5), 7373. doi: 10.1029/92JC00188

Wanninkhof, R. (2014, June). Relationship between wind speed and gas exchange over the ocean revisited: Gas exchange and wind speed over the ocean. *Limnol. Oceanogr. Methods*, *12*(6), 351–362. doi: 10.4319/lom.2014.12.351

Waskom, M. (2021, April). Seaborn: Statistical data visualization. *J. Open Source Softw.*, *6*(60), 3021. doi: 10.21105/joss.03021

Weiss, R. (1974, November). Carbon dioxide in water and seawater: The solubility of a non-ideal gas. *Mar. Chem.*, *2*(3), 203–215. doi: 10.1016/0304-4203(74)90015-2

Wetzel, R. G. (2001). *Limnology: Lake and river ecosystems* (3rd ed.). Elsevier.

White, B., Austin, J., & Matsumoto, K. (2012, March). A three-dimensional model of Lake Superior with ice and biogeochemistry. *J. Great Lakes Res.*, *38*(1), 61–71. doi: 10.1016/j.jglr.2011.12.006

Williamson, C. E., Saros, J. E., Vincent, W. F., & Smol, J. P. (2009, November). Lakes and reservoirs as sentinels, integrators, and regulators of climate change. *Limnol. Oceanogr.*, *54*(6part2), 2273–2282. doi: 10.4319/lo.2009.54.6_part_2.2273

Woolway, R. I., Sharma, S., Weyhenmeyer, G. A., Debolskiy, A., Golub, M., Mercado-Bettín, D., ... Jennings, E. (2021, December). Phenological shifts in lake stratification under climate change. *Nat. Commun.*, *12*(1), 2318. doi: 10.1038/s41467-021-22657-4

Xue, P., Ye, X., Pal, J. S., Chu, P. Y., Kayastha, M. B., & Huang, C. (2022, June). Climate projections over the Great Lakes Region: Using two-way coupling of a regional climate model with a 3-D lake model. *Geosci. Model Dev.*, *15*(11),

4425–4446. doi: 10.5194/gmd-15-4425-2022

Yang, M., Bell, T. G., Bidlot, J.-R., Blomquist, B. W., Butterworth, B. J., Dong, Y., ... Zavarsky, A. (2022, June). Global Synthesis of Air-Sea CO_2 Transfer Velocity Estimates From Ship-Based Eddy Covariance Measurements. *Front. Mar. Sci.*, *9*, 826421. doi: 10.3389/fmars.2022.826421

Young, F. L., Shangguan, Q., Beatty, C. M., Gilsdorf, M. D., & DeGrandpre, M. D. (2022, July). Comparison of spectrophotometric and electrochemical pH measurements for calculating freshwater pCO_2. *Limnol. Oceanogr. Methods*, *20*, 514–529. doi: 10.1002/lom3.10501

Zeebe, R. E., & Wolf-Gladrow, D. A. (2001). *CO_2 in seawater: Equilibrium, kinetics, isotopes* (No. 65). Amsterdam ; New York: Elsevier.

Zigah, P. K., Minor, E. C., Werne, J. P., & McCallister, S. L. (2011, May). Radiocarbon and stable carbon isotopic insights into provenance and cycling of carbon in Lake Superior. *Limnol. Oceanogr.*, *56*(3), 867–886. doi: 10.4319/lo.2011.56.3.0867